Unsteady Aerodynamic Forces on a Vibrating Long-Span Curved Roof

氏　　名	てい　い 丁　威
授与学位	博士（工学）
学位授与年月日	平成 26 年 3 月 27 日
学位授与の根拠法規	学位規則第 4 条第 1 項
研究科，専攻の名称	東北大学大学院工学研究科（博士課程）都市･建築学　専攻
学位論文題目	Unsteady Aerodynamic Forces on a Vibrating Long-span Curved Roof （振動している大スパン曲面屋根に作用する非定常空気力）
指導教員	東北大学教授　植松　康
論文審査委員	主査　東北大学教授　植松　康　　東北大学教授　持田　灯 東北大学教授　五十子　幸樹

論 文 内 容 要 旨

1. Introduction

Wind-structure interaction is a critical consideration in the design of many structures in civil engineering, especially for the structures being flexible and light, such as long-span bridges, high-rise buildings and long-span roofs. Such structures are vulnerable to dynamic wind actions. The wind-structure interaction is represented by the unsteady aerodynamic (or motion-induced wind) forces, which may affect the response significantly. Many researches have been made of the unsteady aerodynamic forces on long-span bridges and high-rise buildings (Taniike et al 1981, Matsumoto et al 1996). The results indicate that unstable vibrations may be induced by negative aerodynamic damping. By comparison, the number of researches on long-span roofs is quite limited. Daw and Davenport (1989) carried out a forced vibration test on a semi-circular roof to investigate the dependence of unsteady aerodynamic forces on the turbulence intensity, wind speed, vibration amplitude and geometric details of the roof. Ohkuma et al. (1990) investigated the mechanism of aeroelastic instability for long-span flat roofs using a forced vibration test in a wind tunnel. At present, however, the characteristics of unsteady aerodynamic forces on long-span curved roofs (vaulted roofs) are not understood well. Therefore, it is necessary to discuss this problem further for proposing more reasonable methods of response analysis of these roofs.

The objective of the present study is to describe the characteristics of unsteady aerodynamic forces acting on a curved roof vibrating in the first anti-symmetric mode. A forced-vibration test is carried out in a wind tunnel. The effects of wind speed, vibration amplitude and frequency on the characteristics of unsteady aerodynamic forces are investigated. However, the range of these parameters involved in the wind tunnel experiment is limited. Therefore, a CFD simulation is carried out to investigate the problem in more detail. In the simulation, the parameters are varied over a wider range. Furthermore, the wind-induced response of real long-span curved roof is evaluated considering the influence of unsteady aerodynamic forces.

2. Description of the Unsteady Aerodynamic Force

The unsteady aerodynamic forces induced by the wind-structure interaction are described. And non-dimensional coefficients, or the aerodynamic stiffness coefficient a_K and aerodynamic damping coefficient a_C are defined by Eqs. (1) and (2) to evaluate the characteristics of unsteady aerodynamic forces:

$$a_{Kj} = \frac{1}{q_H A_s (x_0 / L)} \frac{2}{T} \int_0^T F_j(t) \cos 2\pi f_m t dt \quad ; \quad a_{Cj} = \frac{1}{q_H A_s (x_0 / L)} \frac{2}{T} \int_0^T F_j(t) \sin 2\pi f_m t dt \qquad (1), (2)$$

where q_H = velocity pressure at the mean roof height H; A_s = roof area; x_0 = vibration amplitude; L = span of the roof; and f_m = forced vibration frequency.

3. Wind Tunnel Experiment

3.1 Experimental Arrangement and Procedure

A forced vibration test was carried out in an Eiffel-type wind tunnel. A turbulent boundary layer with a power-law exponent of $\alpha = 0.23$ was generated on the wind tunnel floor. The wind tunnel model is a curved roof as shown in Fig. 1(a). In this figure, *Rs* represents the total length of the curved roof. The experimental setup is shown in Fig. 1(b), which makes the roof vibrate in the first anti-symmetric mode. A pair of end plates is used to generate two-dimensional flow. Each model has 12 pressure taps of 1mm diameter uniformly distributed along the roof's centerline.

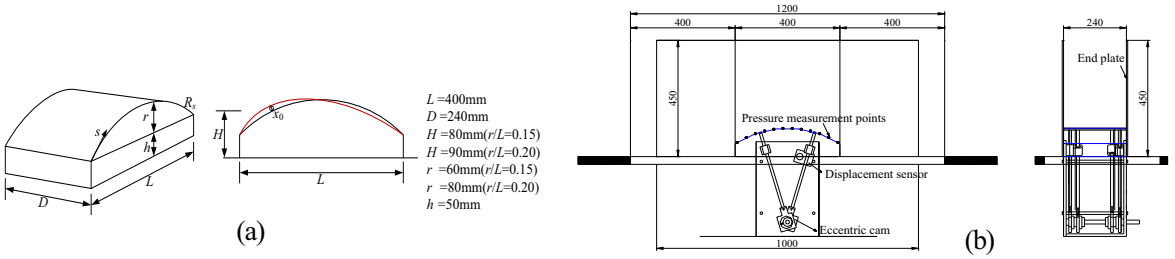

Fig. 1 Experimental model (a) and setup of the forced vibration test (b)

3.2 Results and discussion

Fig. 2 (a) and (b) shows the variation of the aerodynamic stiffness coefficient a_K with the reduced frequency f_m^* (= $f_m H/U_H$) for various wind speeds (a) and vibration amplitudes (b); the rise/span ratio r/L is 0.15. The value of a_K generally increases with an increase in f_m^*. As the reduced frequency decreases, the value of a_K approaches the quasi-steady value (dashed line in the figure). Similar results were observed for r/L=0.20. Within the limits of the present experiment, the value of a_K is generally positive, which may reduce the total stiffness of the structural system resulting in a lower natural frequency. Plotted on Fig. 2 (c) and (d) is the variation of aerodynamic damping coefficient a_C with f_m^* for various wind speeds and vibration amplitudes. The values of a_C are generally negative except for small f^* values, which may increase the total damping of the structural system. The magnitude of a_C increases as the f_m^* value increases. Similar results were observed for r/L=0.20. It can be seen that the effects of wind speed and vibration amplitude on the aerodynamic stiffness and damping coefficients are relatively small and the values of a_K and a_C are mainly dependent on f_m^*.

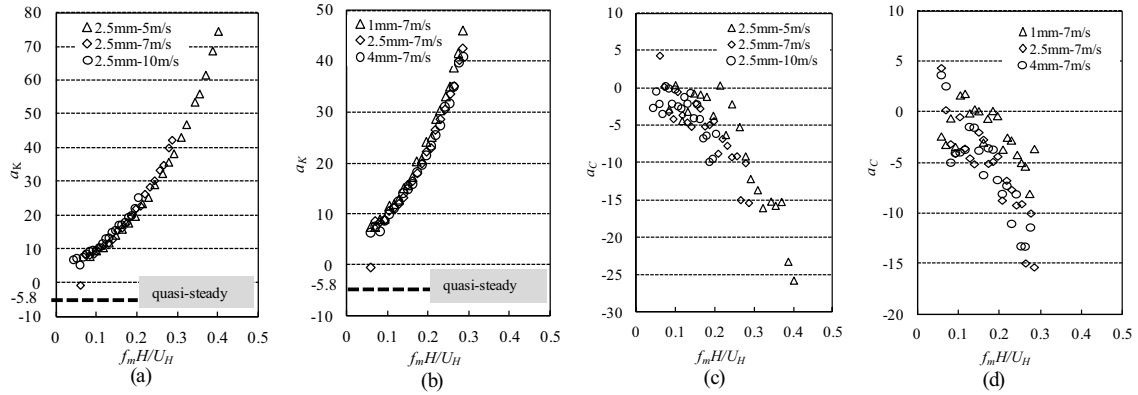

Fig. 2 Aerodynamic stiffness and damping coefficients versus f_m^* (r/L=0.15)

4. CFD Simulation

Because the range of wind tunnel experiment is limited, a CFD simulation is carried out to reproduce the wind tunnel experiment and investigate the characteristics of unsteady aerodynamic forces for a wide range of parameters.

4.1 Computational conditions

A commercial software 'STAR-CD' is used. The large eddy simulation (LES) with the Smagorinsky sub-grid model (C_s=

0.12) is used to simulate the flow field around the model. The computational domain and mesh arrangement are shown in Fig. 3. The inflow turbulence is generated in a preliminary computational domain where roughness blocks are arranged to generate a turbulent boundary layer similar to the wind tunnel flow. The parameter of CFD is summarized in Table 1.

Table 1 Parameter of CFD simulation

Wind speed	5m/s
Forced vibration amplitude	4mm
Rise/span ratio (r/L)	0.15, 0.20, 0.25
Forced vibration frequency (f_m)	0Hz ~160Hz (@10Hz)
Reduced vibration frequency(f^*)	0 ~ 2.5
Inflow	Turbulent flow, Uniform smooth flow

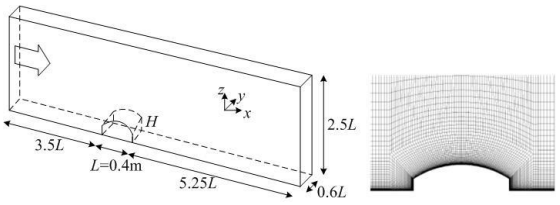

Fig. 3 Computational domain and mesh arrangement

4.2 Computational results

Fig. 4 shows the distributions of the mean wind pressure coefficients along the roof's centerline obtained from the CFD simulation and the wind tunnel experiment, in which the results for the frequencies of 0Hz, 10Hz and 15Hz are plotted. A generally good agreement between these two results can be seen. The difference is somewhat larger near the rooftop; the CFD values are approximately 10% larger in magnitude than the experimental ones. The aerodynamic stiffness and damping coefficients obtained from the CFD simulation and wind tunnel experiment are plotted in Fig. 5. It can be seen that the results of CFD simulation show the same trend with the results of wind tunnel experiment over a wide range of reduced frequency.

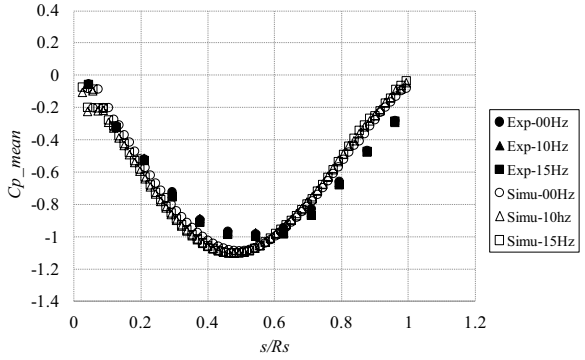

Fig. 4 Comparisons between CFD simulation and wind tunnel experiment for the mean wind pressure coefficient

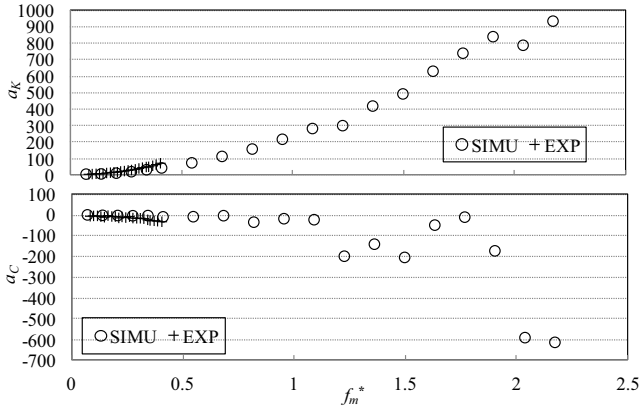

Fig. 5 Comparison of aerodynamic stiffness and damping coefficients between CFD and wind tunnel test

5. Prediction of Wind-induced Response

This section outlines the method for predicting the wind-induced response of a full-scale curved roof to turbulent winds, in which the effects of the unsteady aerodynamic forces are taken into account.

5.1 Theoretical analysis of response

As an example, we consider a long-span membrane structure with the same shape as that used in the wind tunnel experiment. In general, the natural frequency of membrane structure with a span of approximately 100 m is in a range from 0.5 to 1.5 Hz and the mass from 2 to 15 kg/m^2. The wind-induced responses of such structures in a turbulent boundary layer are evaluated based on the aerodynamic stiffness and damping coefficients obtained from the wind tunnel experiments and CFD simulation.

Aerodynamic stiffness (K_{aj}) and aerodynamic damping ratio (ζ_{aj}) are given by Eqs. (3) and (4). The mechanical admittance including the aerodynamic stiffness and damping is defined by Eq. (5). The standard deviation of generalized displacement σ_x is derived from Eq. (6).

$$\frac{K_{a_j}(f)}{K_{s_j}} = -\frac{1}{8\pi^2}\frac{\rho_a}{\rho_{s_j}}\left(\frac{U_H}{f_{s_j}H}\right)^2\frac{H}{L}a_{k_j}(f)\,;\quad \zeta_{a_j}(f) = -\frac{1}{16\pi^2}\frac{\rho_a}{\rho_{s_j}}\left(\frac{U_H}{f_{s_j}H}\right)^2\frac{H}{L}a_{c_j}(f) \qquad (3),(4)$$

$$\left|H_j(f)\right|^2 = \frac{1}{\left[1-\left(\frac{f}{f_{s_j}}\right)^2 + \frac{K_{a_j}(f)}{K_{s_j}}\right]^2 + 4\left(\xi_{s_j}+\xi_{a_j}(f)\right)^2\left(\frac{f}{f_{s_j}}\right)^2} \; ; \quad \sigma_{x_j}^2 = \frac{1}{K_{0_j}^2}\int_0^\infty S_{F_j}(f)\left|H_j(f)\right|^2 df \qquad (5), (6)$$

5.2 Results of wind-induced response

Fig. 6(a) illustrates the mechanical admittance functions plotted against frequency f for various wind speeds, where the structural mass per unit area is assumed 4 kg/m^2. The structural damping ratio ζ_s and the natural frequency f_s of the first anti-symmetric mode are assumed 3 % and 0.5 Hz, respectively. As the wind speed increases, the resonant frequency decreases and the peak value of the mechanical admittance function at the resonant frequency increases. This feature may be due to the effect of positive aerodynamic stiffness coefficient. The variation of mechanical admittance function with the roof's mass is illustrated in Fig. 6(b), in which we assume that U_H = 20m/s. The resonant frequency increases and the resonant peak value of the mechanical admittance function decreases as the roof's mass increases. This feature implies that the increase in mass is quite effective for reducing the aerodynamic excitation of the roof. In other words, the effect of unsteady aerodynamic forces on the response of the roof becomes less significant for heavier roofs.

The relationships between σ_x and U_H were calculated for various roof's masses. Sample results are shown in Fig. 7, in which the natural frequency f_s and the structural damping ratio ζ_s of the roof are assumed 0.5 Hz and 0.05, respectively. It is found that the dynamic response becomes larger with a decrease in the roof mass. Furthermore, the unsteady aerodynamic forces will be less influential on the dynamic responses for heavier roofs, since the dynamic motion dictates the behavior. The dynamic response becomes larger with an increase in the wind speed. The response predicted by considering the effect of aerodynamic forces is larger than that predicted by neglecting the effect of unsteady aerodynamic forces, when the wind speed exceeds a certain value. In other words, the effect of unsteady aerodynamic forces on dynamic responses change from positive to negative as the wind speed increases beyond this value.

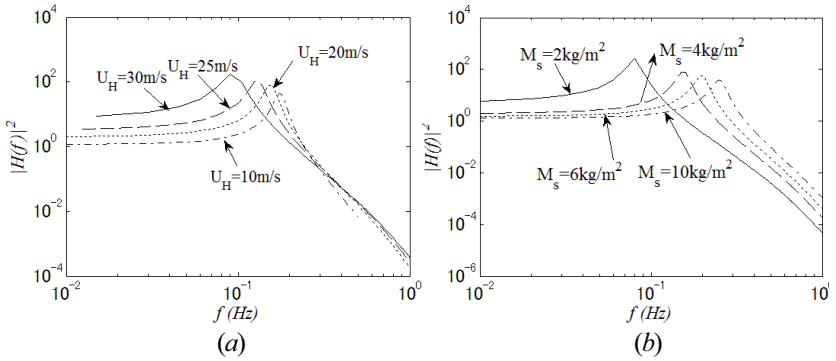

Fig. 6 Variation of mechanical admittance function with wind speed (a) and roof's mass (b)

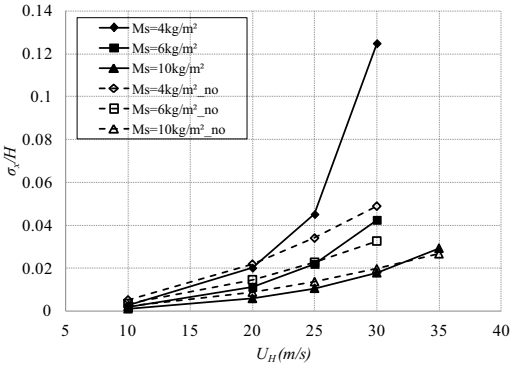

Fig. 7 Variations of standard deviation of generalized displacement (σ_x) with wind speed (U_H)

6. Conclusions

The unsteady aerodynamic force on a long-span curved roof has been investigated based on a wind tunnel experiment as well as on a CFD simulation. The main results obtained from the present study may be summarized as follows:

1) The aerodynamic stiffness and damping coefficients vary with the reduced frequency. The coefficients are minutely influenced by the wind speed, rise/span ratio and vibration amplitude.

2) The general trends of the aerodynamic stiffness and damping coefficients with the reduced frequency obtained from the CFD simulation are consistent with that from the wind tunnel experiment. The value of aerodynamic stiffness coefficient is generally positive, which decreases the total stiffness of the system. On the other hand, the value of aerodynamic damping coefficient is negative, which may result in an increase of the total damping of the system.

3) The unsteady aerodynamic forces reduce the resonant frequency and change the resonant peak. As a long-span curved roof becomes lighter, the effect of the unsteady aerodynamic forces on the dynamic response to turbulent winds becomes more significant. As a result, the wind-induced response of long-span curved roof may increase.

論文審査結果の要旨

本研究は，大スパン屋根の最も一般的な形状である円弧屋根を対象とし，屋根が気流中で振動しているとき，屋根の振動に伴って発生する非定常空気力（振動依存風力）の特性を風洞実験ならびに数値流体計算（CFD）により定量的に把握し，それを屋根の応答評価に取り入れる方法を提案したものであり，全編6章よりなっている。なお，本研究では，非定常空気力とそれが屋根の動的挙動に及ぼす影響の基本的な特性を把握することを主目的としているため，二次元問題のみを扱っている。

第1章は序論であり，本研究の目的と背景，既往の研究概要を述べた。

第2章では，屋根の振動に伴って発生する非定常空気力について理論的な考察を行った。ここで対象としている振動は，空力安定性を論じる上で最も重要となる逆対称1次モードであり，屋根に作用する風力は「1次一般化風力」として評価される。なお，内圧の影響は考慮していない。屋根の振動に伴って発生する付加的な空気力を，屋根の振動変位と同相の成分（空力剛性）と振動速度と同相の成分（空力減衰）の線形和として近似的に表現し，それぞれを無次元化した「空力減衰係数」a_Kと「空力減衰係数」a_Cを独自に定義し，構造物の剛性係数や減衰定数と直接比較できるようにした。

第3章では，屋根に逆対称1次モードの強制振動を与えられる強制加振装置を独自に設計・製作し，風洞気流（境界層乱流）中で屋根を一定振幅・一定振動数で強制加振しながら屋根に作用する変動風圧の多点同時測定を行った。屋根のライズ・スパン比（r/L）は0.15と0.2の2種類であり，それぞれに対し，屋根平均高さでの風速U_H，加振動振幅x_0，加振振動数f_mを変化させた。実験結果に基づき，空力剛性係数a_Kと空力減衰係数a_Cを計算し，無次元振動数f_m^*（$=f_mH/U_H$）に対してプロットした。一般に，a_Kは正であり，構造物の見かけの剛性を低下させて振動を増大させる作用をするのに対し，a_Cは負であり，構造物の見かけの減衰を増大させて振動を安定化させる作用をすることを見出した。また，a_Kおよびa_Cの大きさは，いずれもf_m^*の増大に伴い増大するが，U_H，x_0，f_mの影響は比較的小さいことを示した。

第4章では，先ず第3章で実施された風洞実験をLES（Large Eddy Simulation）を用いた数値流体計算で模擬し，流入変動風と乱流パラメータの値を適切に設定することで，風洞実験結果を概ね再現できることを確認した。風洞実験では装置や時間の制約のため検討できる条件が限定されてしまうので，それを補完し，より広範囲のデータを得ることを目的に一連のCFD解析を実施した。ライズ・スパン比は，実験で検討した0.15と0.2のほか0.25を加えた。無次元振動数f_m^*も，実験では0～0.4程度に限られていたが，約2まで拡大した。さらに，気流の乱れの影響をみるため，境界層乱流に加え一様流も用いた。一連のCFD解析により，実用的な範囲で非定常空気力の特性を把握することができた。

第5章では，第4章の結果に基づきa_Kおよびa_Cのモデル化を行い，構造物の風応答解析において一般に使用されるスペクトルモーダル解析の枠組みの中にそれらを取り入れ，非定常空気力の効果を考慮した応答解析手法を提案した。また，代表的なモデルを設定して系統的な解析を行い，屋根の動的応答に及ぼす屋根の質量や剛性の影響を示した。

第6章は結論であり，本研究で得られた主な結論をまとめた。

以上，要するに本論文は，大スパン円弧屋根を対象とし，振動に伴って発生する非定常空気力の特性を風洞実験並びに数値流体計算に基づき明らかにし，屋根の空力安定性を論じるとともに，非定常空気力を考慮した動的応答評価手法を提案したものであり，今後の大スパン構造の耐風安全性や合理的な応答評価・耐風設計に寄与するところが大きい。

よって、本論文は博士（工学）の学位論文として合格と認める。